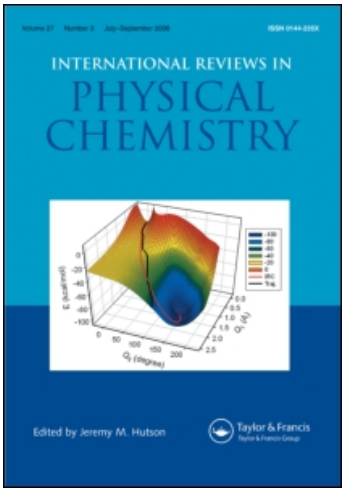

International Reviews in Physical Chemistry
Publication details, including instructions for authors and subscription information:
http://www.informaworld.com/smpp/title~content=t713724383

Diffusion Monte Carlo approaches for investigating the structure and vibrational spectra of fluxional systems

Anne B. McCoy[a]
[a] Department of Chemistry, The Ohio State University, Columbus, OH 43210, USA

Online publication date: 28 November 2010

To cite this Article McCoy, Anne B.(2006) 'Diffusion Monte Carlo approaches for investigating the structure and vibrational spectra of fluxional systems', International Reviews in Physical Chemistry, 25: 1, 77 — 107
To link to this Article: DOI: 10.1080/01442350600679347
URL: http://dx.doi.org/10.1080/01442350600679347

International Reviews in Physical Chemistry,
Vol. 25, Nos. 1–2, January–June 2006, 77–107

Taylor & Francis
Taylor & Francis Group

Diffusion Monte Carlo approaches for investigating the structure and vibrational spectra of fluxional systems

ANNE B. McCOY*

Department of Chemistry, The Ohio State University, Columbus, OH 43210, USA

(*Received 7 March 2006*)

Recent advances in diffusion Monte Carlo (DMC) are reviewed within the context of the vibrational motions of systems that undergo large amplitude motions. Specifically, the authors describe the DMC approach for obtaining the ground state wave function and zero-point energy (ZPE) of the system of interest, as well as extensions to the method for evaluating probability amplitudes, rotational constants, vibrationally excited states and methods for obtaining vibrational spectra. The discussion is framed in terms of the properties of several systems of current experimental and theoretical interest, specifically complexes of neon atoms with OH or SH, $H_3O_2^-$, $H_5O_2^+$, and CH_5^+. The results of the DMC simulations provide the information necessary to characterize the extent of delocalization of the probability amplitudes, even in the ground vibrational states. Methods for evaluating expectation values and vibrationally excited states are explored, and, when possible, the results are compared with those from other approaches. Finally, the methods for evaluating intensities are described and existing and future challenges for the approach are reviewed.

Contents

*Email: mccoy@chemistry.ohio-state.edu

International Reviews in Physical Chemistry
ISSN 0144–235X print/ISSN 1366–591X online
http://www.tandf.co.uk/journals
DOI: 10.1080/01442350600679347

1. Introduction

A significant challenge in chemical physics appears in making connections between the positions and intensities of vibrational transitions, observed through spectroscopic measurements, and properties of molecules. For molecules that undergo small amplitude vibrations near an equilibrium configuration, normal mode treatments, or perturbation theory based on a zero-order normal mode representation of the vibrational Hamiltonian, have been shown to be extremely effective [1, 2]. On the other hand, highly anharmonic species that undergo large amplitude vibrational motions are not well suited for such an approach as the zero-point energy (ZPE) often exceeds the barriers that separate minima on the potential. Classic examples of such systems are complexes that are held together by van der Waals or hydrogen bonding interactions. Even the simplest of these complexes explore a large range of angular motion when the complex is in its ground vibrational state. For example, the ground state of ArHF has non-zero amplitude in the Ar–FH as well as the Ar–HF minima on the H6(4,3,2) potential of Hutson [3, 4]. As the complexes become larger or the molecules that comprise them become non-linear, the number of minima increases as can the delocalization of the ground state wave function. In addition to being highly fluxional, the fact that they are held together by weak intermolecular interactions, places the dissociation energy at several kilocalories per mole. This often results in the zero-point level sampling highly anharmonic regions of the potential.

A second class of systems that has received considerable attention recently are molecular ions like $H_3O_2^-$, $H_5O_2^+$, and CH_5^+. In contrast to the van der Waals systems, these ions are bound by 25, 32, and 40 kcal mol^{-1}, relative to the dissociation products of $H_2O + OH^-$ [5], $H_2O + H_3O^+$ [6], and $CH_3^+ + H_2$ [7], respectively. On the other hand, all three display large amplitude vibrational motions in their ground states. They are of particular interest due to their importance in interstellar chemistry as well as important intermediates in aqueous chemistry. They have also been subjected to spectroscopic studies of the vibrational spectra in the 600–3800 cm^{-1} region [8–17]. High-resolution, rotationally resolved spectra in the 2800–3100 cm^{-1} region

have been reported for CH_5^+ [18, 19]. There has also been considerable theoretical and computational work performed on all of these species. A thorough review of that work is beyond the scope of the present review, and readers are referred to [20] for a recent discussion of work on CH_5^+ and to [21] for a review on protonated water clusters.

As we consider the theoretical and computational approaches that can be used to investigate vibrational energy levels and wave functions, the most powerful approaches are those based on the variational theorem. Large-scale variational calculations of systems with more than four atoms and that sample multiple minima on the potential surface, even in their ground states, are approaching or exceeding our current capabilities. In addition, even if one can obtain an *exact* solution to the time-independent Schrödinger equation, interpreting the massive amounts of numerical data can be challenging. That said, the MULTIMODE approach of Bowman and co-workers [22], has been applied to studies of the vibrational motions of CH_5^+, $H_5O_2^+$, and $H_3O_2^-$ [19, 23–28]. The cc-VSCF approach of Gerber and co-workers has been applied to complexes of water molecules with Cl^-, H^+, and F^- [29, 30].

An alternative approach for investigating the vibrational ground state of an arbitrary molecular system is the diffusion Monte Carlo (DMC) method [31]. This method employs a Monte Carlo approach for solving the imaginary-time, time-dependent Schrödinger equation. In contrast to the variational approaches, this method does not employ a basis set and as a result is ideally suited for systems like those mentioned earlier, for which there does not exist an obvious zero-order description of the vibrations in terms of a direct product basis. While DMC is entirely general, it suffers from the fact that it relies on imaginary-time propagations to generate the ground state wave function and ZPE of the system of interest. This makes studies involving rotationally or vibrationally excited states less straightforward.

In this review, the focus is on extensions and modifications to the DMC approach. These are discussed in the context of the three molecular ions, $H_3O_2^-$, H_5O_2+ and CH_5^+, as well as complexes of neon atoms with OH or SH. The DMC studies of larger rare gas clusters, in particular those involving doped helium droplets [32], as well as neutral water clusters [33–36], and complexes of rare gas atoms with closed-shell species [37] have been reported over the past several years. In addition, extensive work has been performed to apply these approaches to electronic structure problems. The work in this area has been reviewed in the *Recent Advances in Quantum Monte Carlo* [38, 39] series of books.

2. Systems

Before describing the DMC approaches, the systems that are used to illustrate these approaches are briefly reviewed.

2.1. *$Ne_n \cdot XH$ complexes*

The spectroscopy of complexes of rare-gas atoms with OH or SH was reviewed by Carter *et al.* in 2000 [40] and more recently by Heaven [41]. In the studies presented here, the $Ne_n \cdot XH$ complexes are modeled by pair-wise sums of Ne–Ne interactions

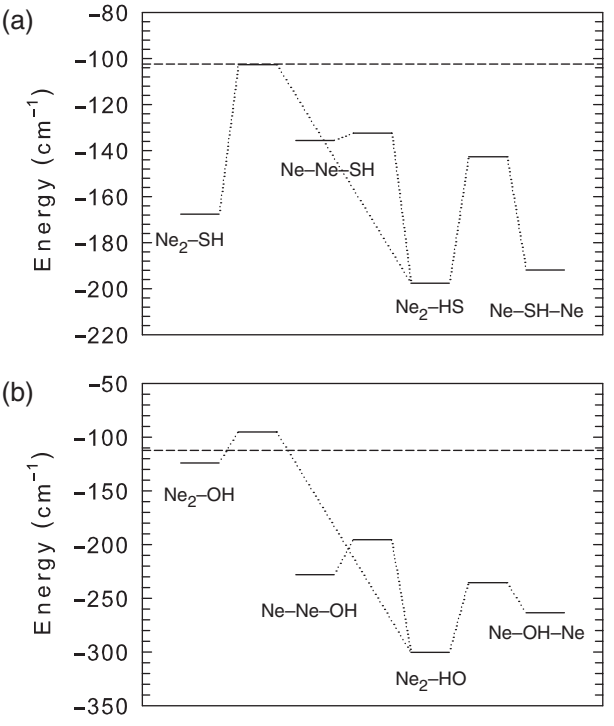

Figure 1. Energies of low-lying stationary points on the (a) Ne_2SH and (b) Ne_2OH potentials. The ZPEs of these systems are plotted with dashed lines.

[42] and Ne–XH interactions [43, 44]. To illustrate the range of motions of these complexes, in figure 1 we plot the energies of various stationary points on the Ne_2XH $\tilde{A}$–state potentials. For calibration, the ZPEs of the complexes are plotted with dashed lines. In both of the systems, the minimum energy structure is *T*-shaped with the XH pointing at the center of the neon dimer. We focus on these systems as they are the ones for which we have also performed fully converged variational calculations [45]. As such, they provide a point of comparison for the DMC methods.

2.2. *$H_3O_2^-$ and $H_5O_2^+$*

Both $H_3O_2^-$ and $H_5O_2^+$ are chemically more interesting species as they provide examples of the smallest possible aqueous complexes of the hydroxide and hydronium ions. For $H_3O_2^-$, the best available surface is one that was obtained by Bowman and co-workers at the CCSD(T)/aug-cc-pVTZ level of theory/basis. This potential is based on 66 965 electronic energies that were fit to a high-order expansion in functions of the atom–atom distance coordinates [25]. More recently, this surface has been extended to provide a global surface that allows for dissociation to OH^- and H_2O [27]. In the case of $H_5O_2^+$, several surfaces have been used for DMC studies. Until recently, the best available surface for this system was the OSS3(p) [46, 47] surface of Ojame,

Shavitt, and Singer. This surface has been used by Cho and Singer [23, 48] for DMC simulations of $H_5O_2^+$, while an earlier version of the surface was used in DMC studies by Buch [49] and co-workers and by Mella and Clary [36] in the studies of $H_5O_2^+$, its deuterated analogues and larger protonated water clusters. In our DMC studies of $H_5O_2^+$, we employed the potential of Huang *et al.* [50]. As for $H_3O_2^-$, this potential is a fit of 48 189 electronic energies, calculated at the CCSD(T)/aug-cc-pVTZ level of theory/basis, to a polynomial expansion in functions of the atom–atom distances.

Based on this potential for $H_3O_2^-$, as well as electronic structure calculations [5, 51], the minimum energy structure has the central hydrogen slightly closer to one of the two oxygen atoms, as is depicted in figure 2(a). There is a low-lying saddle point, in the center of figure 2(a), in which the central hydrogen is equidistant from the two oxygen atoms. As this saddle point is only $68.5\,cm^{-1}$ above the global minimum on the potential surface used in our calculations [27], and the normal mode that roughly connects the minimum to this saddle point has a frequency of $1569\,cm^{-1}$, or 23 times the barrier height, it is anticipated that even in the vibrational ground state, the probability amplitude will be delocalized across this barrier [51]. In addition, there is a low-frequency torsion mode, which corresponds to the HOOH torsion and is analogous to the corresponding motion in hydrogen peroxide. The barriers in the *cis*- and *trans*-configuration are 376 and $166\,cm^{-1}$ above the potential minimum [25]. Again, it is anticipated that the ground vibrational state will be highly delocalized in this coordinate.

To approximate the extent of delocalization, we compute the harmonic ZPE at each stationary point, where we take this quantity to be half the sum of the real frequencies at each configuration. The differences between the sum of the potential energy at the saddle points and the corresponding ZPE and the ZPE at the potential minimum are plotted with dashed lines. As is seen, when zero-point effects are included in this way, the minimum energy structure corresponds to the one in which the central hydrogen is equidistant from the two oxygen atoms. This structure is often referred to as the *Zundel* structure [52]. In addition, the *trans*-barrier height drops to $80\,cm^{-1}$, less than half of the $206\,cm^{-1}$ torsion frequency at the potential minimum. The *cis*-barrier also drops, to $318\,cm^{-1}$, but this one is considerably above the torsion frequency. The above considerations lead to the expectation that the ground state wave function will have a significant amplitude in the Zundel structure as well as across the *trans*-barrier, but will be small in the region of the *cis*-barrier. These expectations are borne out in the projections of the DMC probability amplitudes onto these coordinates [27].

The equilibrium structure of $H_5O_2^+$ is shown in figure 2(b). In contrast to $H_3O_2^-$, the minimum energy structure of $H_5O_2^+$ has the central hydrogen equidistant from both oxygen atoms and the OHO is nearly linear, e.g. the Zundel structure. For this system, the low-frequency motions correspond to the inversion motions of the two water groups. These can be thought of as being analogous to the inversion mode in H_3O^+ or more familiarly in NH_3. The barrier for this motion at one end of the ion is $164\,cm^{-1}$, $98\,cm^{-1}$ with ZPE included. There is also a low-frequency torsional mode. Here the barriers along this coordinate are 213 and $434\,cm^{-1}$ in the *trans*- and *cis*-configurations, respectively. They drop to 154 and $267\,cm^{-1}$, when ZPE is included. As Wales has pointed out [53], the topology of this potential is complicated by the

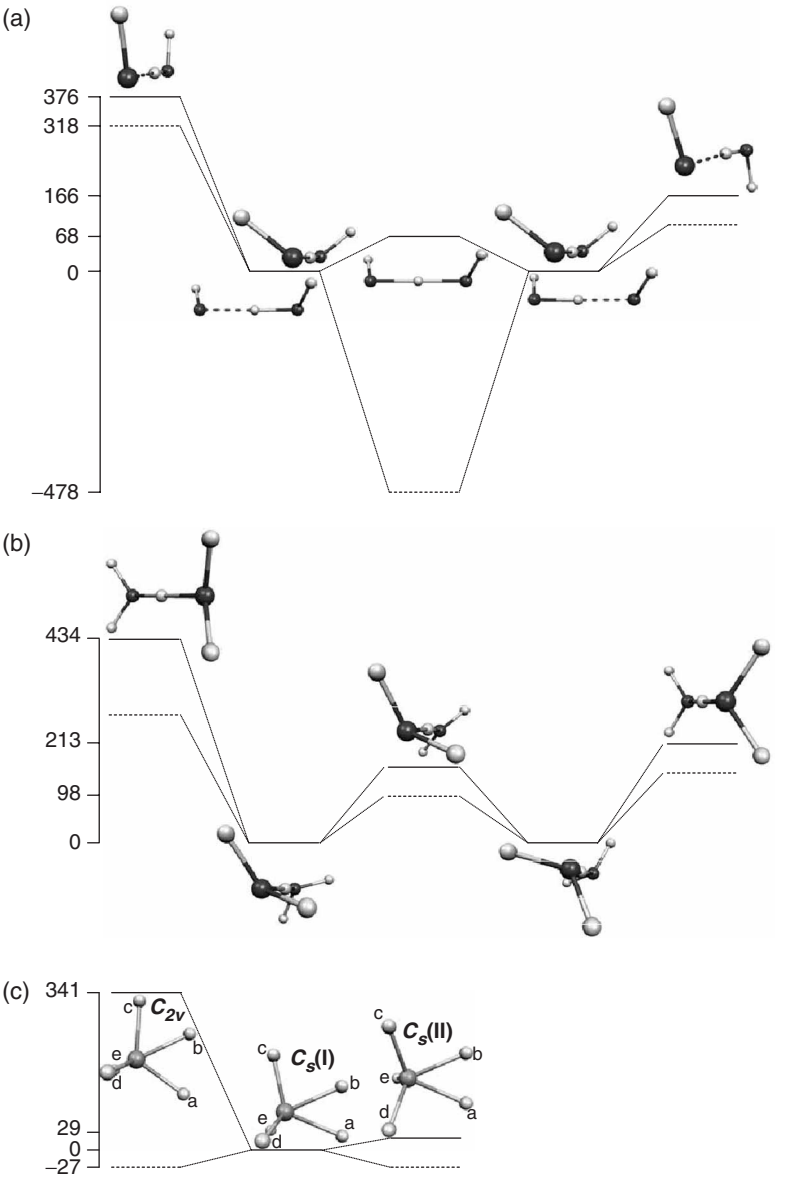

Figure 2. Energies and structures of low-lying stationary points on the (a) $H_3O_2^-$ [25], (b) $H_5O_2^+$ [25] and (c) CH_5^+ [7]. Solid lines provide the energies on the potential surfaces. Dashed lines give the sum of the electronic energy and the harmonic ZPE at these points. All plots are shown on the same energy scale and the energies are reported in cm^{-1}. The energy at the potential minimum is zero.

fact that the two minimum energy configurations can be connected either through the low-energy flipping barriers or by torsion motion.

As is demonstrated by the above discussion, both $H_3O_2^-$ and $H_5O_2^+$ have multiple low-lying potential minima, connected through low-energy barriers, making them good candidates for the DMC treatments.

2.3. CH_5^+

The final system we use to illustrate DMC approaches is CH_5^+. This system has been of extensive and long-term interest both due to its importance in interstellar chemistry [54], and as the simplest of the carbocations [55]. While it has been investigated spectroscopically by a number of groups, its high resolution spectrum has not, as yet, been assigned, although the features in a recently reported lower-resolution spectrum can be understood [9, 19, 26]. As with the water systems, we use a non-global version of the surface of Bowman and co-workers [7, 56, 57]. The potential is a polynomial fit of many electronic energies, calculated at the CCSD(T)/aug-cc-pVTZ level of theory/basis. This surface reflects the full permutation/inversion symmetry of CH_5^+.

The minimum energy structure of CH_5^+ is shown in the middle figure 2(c) and will be referred to as the C_s(I) structure. It has C_s symmetry with three of the hydrogen atoms lying in the same plane as the carbon atom. They have been labeled a, b and c. The remaining two carbon atoms are symmetrically arranged above and below this plane and are labeled d and e. Examination of the equilibrium geometry shows that the hydrogen atoms labeled c–e are roughly equidistant from the carbon atom, with CH distances ranging from 1.088–1.108Å, while the hydrogen atoms labeled a and b are 1.197 Å from the carbon atom [7]. This difference in the bond lengths, reflecting differences in bonding, has led workers to consider CH_5^+ as a CH_3^+ unit, bonded to a H_2 through a three-centered, two-electron bond [58].

Since there are five carbon atoms, there must be 120 equivalent minima on this potential. It can be shown that all of these minima can be connected through two low-lying saddle points. The lower energy one is shown in figure 2(c) and referred to as the C_s(II) structure. Here the atoms are labeled to show the relationship between this saddle point and the minimum energy structure. Examination of these two structures shows that the motion between the C_s(I) and C_s(II) structures corresponds to a 30° rotation of the $H_a - H_b$ sub-unit. While different levels of theory and different calculations predict slightly different energies for the C_s(II) saddle point, they all predict it to be small and range from 30–50 cm^{-1} above the global minimum [58]. The surface used here predicts this barrier to be at 29 cm^{-1} [7].

The second low-lying saddle point is shown on the left in figure 2(c) and is referred to as the C_{2v} structure. Again, the hydrogen atoms are labeled with the letters a–e. Comparison of this structure and the one with minimum energy shows that the motion across the C_{2v} saddle point corresponds to flipping of H_b between H_a and H_c, and rendering the hydrogen atoms labeled b and c the H_2 unit. This barrier has been calculated to be between 100 and 400 cm^{-1} [58], and is 341 cm^{-1} on the potential used in the present study. When harmonic ZPE is introduced, these two saddle points become lower in energy than the potential minimum by 26 cm^{-1} (C_s(II)) and 27 cm^{-1}(C_{2v}).

Based on the above discussion, it has been anticipated that the ground state of CH_5^+ will be delocalized among all 120 equivalent minima with substantial probability amplitude at the C_s(II) and C_{2v} structures. While outside the scope of the present discussion, this localization will be quenched upon deuteration. This was first predicted by Marx and Parrinello [59] from their path-integral calculations and is seen experimentally in the studies of Lee and co-workers on complexes of CH_5^+ with H_2 [8]. More recently, we have demonstrated this by the DMC approaches [60, 61].

Again, ours are not the only DMC studies that have been performed on this species. Jordan and co-workers reported studies of CH_5^+ at the same time as our original reports [62]. While they used a somewhat different potential surface, the overall picture obtained in their and our studies is nearly identical.

3. Ground state wave functions and energies

3.1. *Theory*

While there are a number of formulations of DMC and a number of ways in which the simulations may be preformed, the simplest statement of the approach and its implementation can be found in the original description by Anderson [63, 64]. An excellent review of the approach was given by Suhm and Watts [65]. It includes many of the important aspects of the method. The basic idea starts with the general solution to the time-dependent Schrödinger equation,

$$|\Psi(t)\rangle = \sum_n c_n e^{-iE_n t/\hbar}|n\rangle \tag{1}$$

where the c_n are the expansion coefficients at $t=0$ and

$$\hat{H}|n\rangle = E_n|n\rangle. \tag{2}$$

While the solution to the time-dependent Schrödinger equation is an oscillatory function of time, and if we replace t with $\tau = it/\hbar$, equation (1) becomes

$$\Psi(\tau) = \sum_n c_n e^{-E_n\tau}|n\rangle \tag{3}$$

and, at long times, the sum will be dominated by the lowest energy eigenstate. The decay of the amplitude is related to the ZPE of the system. It should be noted that Kosloff and Tal-Ezer have exploited this relationship to obtain the quantum mechanical ground state from time-dependent simulations [66]. It should also be noted that there is nothing related to diffusion or Monte Carlo in the above discussion.

Both the above aspects come into the method employed to solve the imaginary-time, time-dependent Schrödinger equation. First, we rewrite the time-dependent Schrödinger equation as a propagator,

$$\left|\Psi(\tau+\Delta\tau)\right\rangle = e^{-(\hat{H}-E_0)\Delta\tau}\left|\Psi(\tau)\right\rangle \tag{4}$$

where, to simplify the discussion that follows, we shift the zero-in energy by the ZPE of the system of interest. This can be approximated by

$$\left|\Psi(\tau+\Delta\tau)\right\rangle \approx e^{-(\hat{V}-E_0)\Delta\tau}e^{-\hat{T}\Delta\tau}\left|\Psi(\tau)\right\rangle \tag{5}$$

This is the simplest form of the split-operator of Feit and Fleck [67] which has been shown to be accurate for small time-steps.

As mentioned above, for DMC simulations one does not employ a traditional basis-set approach, but instead the goal is to generate a Monte Carlo sampling of the ground state wave function. As such, the wave function will be represented by an ensemble of δ-functions, or walkers. Next, to keep the simulation as simple as possible, it will be assumed that the kinetic energy takes the form,

$$\hat{T} = \sum_{i=1}^{n} -\frac{\hbar^2}{2m_i}\frac{\partial^2}{\partial q_i} \tag{6}$$

where, in most of the cases considered here, the sum is over the $n=3N$ Cartesian coordinates of the N-atomic system and q_i represents one of the Cartesian coordinates of one of the atoms. In the case of the complexes of neon atoms with SH or OH, we treat the diatomic molecule as a rigid rod and the coordinates of the hydrogen and oxygen/sulfur atoms are replaced by the center of mass motion of SH or OH and three angles that define the orientation of SH or OH with respect to a space-fixed axis system. Details of this so-called rigid-body DMC approach are not presented here, but can be found in the work of Buch and co-workers [68]. In this approach, the Cartesian coordinates are replaced by angles of rotation about a principal axis system and the masses are replaced by the corresponding moments of inertia. A procedure for implementing this is given in [69]. The same result can be achieved by using 'quaternions' and such an approach has been described by Benoit and Clary [70].

Independent of whether the kinetic energy operator is written in terms of Cartesian coordinates alone or combinations thereof and rotation angles, assuming that the kinetic energy operator is separable, its action on each of the coordinates can be considered independently. Further, if we treat our walkers as n-dimensional δ-functions, one finds that the action of the kinetic propagator on a δ-function yields a Gaussian with a width given by

$$\sigma_i = \sqrt{\frac{\Delta\tau}{m_i}}. \tag{7}$$

As such, at each time-step we move each of the n coordinates by an amount that, when averaged over all the walkers in the ensemble, is consistent with a Gaussian distribution with a width σ_i. This provides the 'diffusion'. The first part of the Monte Carlo aspect of DMC comes from the fact that the size of each step is taken from a Gaussian-random distribution. The second part of the propagator involves the potential

energy. If, at the coordinates of a particular walker, the potential energy is larger than E_0, the walker is in a classically allowed portion of the potential, and $\exp[-(V(x) - E_0)\Delta\tau] > 1$. On the other hand, the exponential will be smaller than one if the walker is in a classically forbidden region of the potential. There are two ways to handle this term. One is the so-called continuous weighting scheme in which the importance, or weight, of a given walker is multiplied by $\exp[-(V(x) - E_0)\Delta\tau]$ at each time-step. This approach suffers from the fact that after a long propagation time, a small fraction of the walkers can carry most of the total weight. An alternative is the so-called branching approach in which all the walkers are required to have equal weights throughout the simulation. In this approach, the integer value of $\exp[-(V(x) - E_0)\Delta\tau]$ provides the number of walkers at that geometry. An additional walker is created at that configuration if the fractional part of $\exp[-(V(x) - E_0)\Delta\tau]$ is larger than a random number, chosen from a uniform distribution on the range (0,1).

As stated above, this procedure provides a Monte Carlo sampling of the ground-state wave function, but requires knowledge of E_0. Following the early work of Anderson [63], we approximate E_0 by

$$W(\tau) = \overline{V} - \alpha \frac{N(\tau) - N(0)}{N(0)} \tag{8}$$

Here $\overline{V}$ is the ensemble average of the potential. This quantity will fluctuate as the walkers move during the simulation. The second term is introduced to ensure that the number of walkers remain roughly constant. Here $N(\tau)$ represents the number of walkers at imaginary-time, τ. If there are more walkers at time τ then when $\tau = 0$, this term will have the effect of decreasing $W(\tau)$ and thereby killing off some of the walkers. Conversely, if the population has declined, this term will increase $W(\tau)$ and lead to more walkers being generated after the next time-step. The value of α is typically close to $1/\Delta\tau$. Operationally, we find it is best to choose α so that the large amplitude fluctuations in $W(\tau)$ occur over 10–20 time steps [65].

3.2. *Results*

As implied by the foregoing discussion, no approximations have been made in computing the ZPE of a system of interest. Errors are introduced from the statistical simulations, but by watching the dependencies of the energy on $\Delta\tau$, on α, and on the ensemble size, one can obtain reasonable estimates of the statistical uncertainties. In this section, we present the results for several systems for which the ZPE can be computed variationally. We also present comparisons to the results of MULTIMODE calculations [22] on $H_5O_2^-$, CH_5^+, and $H_3O_2^-$ and their deuterated analogues, which provide variational upper bounds to the 'true' ZPE of the system of interest. More detailed accounts of these studies can be found in the original work.

Before considering the results, it is useful to look at the results that are obtained from a single DMC simulation. In figure 3, W is plotted as a function of τ for a simulation of CH_5^+ in which all of the walkers are initially placed in the same configuration, obtained

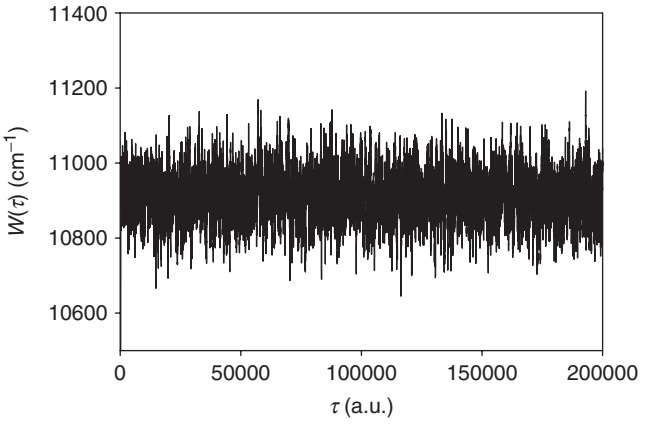

Figure 3. Sample plot of the ZPE, plotted as a function of τ for the ground state of CH_5^+. For this simulation, we used $\alpha = 0.01$ Hartree, $\Delta\tau = 10i$ a.u. At $\tau = 0$, the Cartesian coordinates of all the atoms are 1.1 times their values at the equilibrium, in a center of mass frame.

by multiplying the Cartesian coordinates at equilibrium by 1.1. An ensemble of 20 000 walkers was used for this calculation, $\Delta\tau = 10i$ in atomic units, and $\alpha = 0.01$ Hartree. As can be seen, it takes a small number of time-steps to equilibrate the system, after which time the fluctuations within this simulation are quite large. On the other hand, if we average the energy over the final 15 000 time-steps of the simulation and take the average of the resulting quantities for six simulations, which range from 10 905 to 10 913 cm^{-1}, we obtain an average ZPE of 10 908 cm^{-1} and a standard deviation of 2 cm^{-1}. For comparison, large MULTIMODE calculations provide a ZPE of 10 989 cm^{-1} [61]. This difference may seem large. As mentioned earlier, CH_5^+ is a particularly challenging system for basis-set approaches, and, as indicated in figure 2, the ground state is expected to be highly delocalized. When CH_5^+ is partially deuterated, the ground state wave function becomes localized [59–61] in a smaller fraction of the 120 equivalent minima and connecting saddle points. This is purely a quantum mechanical effect and reflects the inequivalence of the various binding sites, shown in figure 2(c). The MULTIMODE and DMC zero-point energies of all six isotoplogues are compared in table 1. Focusing the energies of CH_5^+, we note that the smallest difference between the two calculations of the ZPE is found for CHD_4^+. Here the MULTIMODE energy is only 32 cm^{-1} above the DMC one. For this species, analysis of the DMC ground state wave function shows that nearly 75% of the probability amplitude is contained in the minimum in which hydrogen is in position d and in the saddle points that are directly connected to that minimum [26]. As CH_5^+ is an extreme case, in terms of the amount of configuration space that is sampled by the ground state wave function, the level of agreement is quite remarkable.

Comparisons of the zero-point energies for several other four- to seven-atomic systems are reported in table 1. As seen, for the systems with four atoms, the energies agree within the stated uncertainty of the DMC simulation. In other cases, the DMC energies are lower than the MULTIMODE ones, as expected. The differences are smaller for the smaller systems, which is not surprising given the difficulty of

Table 1. Comparison of DMC and variational energies.

System	E_{DMC}[a]	E_{var}	Ref.
Ne_2OH	−112.4 (0.2)	−112.2	45, 71
Ne_2SH	−102.4 (0.1)	−102.3	45, 69
H_3O^+	7445 (10)	7451[b]	72
H_2O_2	5725 (3)	5726	28, 73
D_2O_2	4326 (3)	4326	28, 73
$H_3O_2^-$	6605 (5)	6625[b]	27
$D_3O_2^-$	4877 (5)	4882[b]	27
CH_5^+[c]	11 102 (14)		62
CH_5^+	10 908 (5)	10 989[b]	26, 61
CH_4D^+	10 298 (5)	10 359[b]	26, 61
$CH_3D_2^+$	9690 (5)	9733	61, 74
$CH_2D_3^+$	9090 (5)	9149	61, 74
CHD_4^+	8559 (5)	8591[b]	26, 61
CD_5^+	8039 (5)	8083[b]	26, 61
$H_5O_2^+$[d]	12 222 (1)	12 321	24, 48
$H_5O_2^+$	12 393 (5)	12 539[b]	28, 74

[a] Numbers in parentheses represent the uncertainties in the DMC energies.
[b] E_{var} are calculated using MULTIMODE details are provided in the references.
[c] Based on the surface of Thompson *et al.*
[d] Based on the OSS3(p) surface [46].

full-dimensional variational calculations on fluxional molecules with six or seven atoms. The agreement tends to be better for the deuterated species, with differences that are disproportionately smaller in $D_3O_2^-$, compared to $H_3O_2^-$, and for CD_5^+ compared to CH_5^+. This probably reflects the greater localization of the wave function upon deuteration. Interestingly, when we consider vibrationally excited states for $H_3O_2^-$ and $D_3O_2^-$, the trend will be reversed.

The agreement for $H_5O_2^+$ is poorer than for the other systems. This reflects the fact that this system has seven atoms, or fifteen vibrational degrees of freedom. As is shown in figure 2 it also has three first-order saddle points with energies below $500\,cm^{-1}$. There are two additional higher-order saddle points with energies between 500 and $1000\,cm^{-1}$ [50]. The size of the system and the amount of configuration space it can sample, even in its ground state, put $H_5O_2^+$ and $D_5O_2^+$ close to or above the limits of currently available basis-set based approaches and defines the boundary where quantum mechanical approaches, like DMC, that do not require a basis set provide the best alternative, at least at present.

For CH_5^+ [62] and $H_5O_2^+$ [36, 48, 49], DMC simulations have been performed on different potential surfaces than were used in our work. Not surprisingly, the zero-point energies depend on the potential that is employed. The results of these calculations were included in table 1 to illustrate that the DMC (and other vibrational calculations) require a potential surface, and no matter how accurate the vibrational calculations are, the final results and the agreement with experiment will depend sensitively on the quality of the potential that is used. With developments in electronic structure codes and in computers, as well as systematic approaches for generating potentials from electronic energies, significant progress is being made in these directions. Two such approaches have been applied to the studies of CH_5^+ [57, 62].

4. Obtaining properties from DMC

In addition to providing information about the ZPE, DMC provides a Monte Carlo sampling of the ground state wave function. While this cannot and should not be confused with the probability amplitude, which will be needed to obtain expectation values, it can be useful on its own, for example, for obtaining overlaps with the functions that can be expressed analytically [75]. On the other hand, many properties of interest require the ability to average over $|\Psi|^2$, rather than the wave function. In the discussion that follows, we describe three approaches for achieving this. These are not the only approaches that have been used. For example, Broude and Gerber employed a fitting procedure to obtain analytical representations for their wave functions for $Hg(H_2)_{12}$ and $Mg(H_2)_{12}$ clusters [76].

4.1. *Averaging by Pair Counting (AVPC)*

As one considers ways to obtain $|\Psi|^2$, an obvious solution is to replace each of the walkers with an n-dimensional Gaussian with a small, but finite width in each coordinate. This gives a form for the wave function that can be evaluated readily. While this approach is straightforward on paper, it is not particularly useful since a single simulation often has on the order of 20 000 walkers and one needs to average the results over several representations of the wave function. Sandler, Buch, and Sanlej found that replacing the Gaussian by n-dimensional hyper-sphere and counting the number of overlapping spheres provides an alternative way to convolute the wave function [77], but even here, the calculations are expensive. A second issue comes in the radius of the hyper-sphere. If it is too small, the simulation becomes numerically unstable, while too large a radius artificially broadens the wave function, introducing errors. For these above reasons, we have only pursued this approach when others are not available, for example, for evaluating overlaps of ground state and excited state wave functions in order to obtain intensities, an application introduced by Severson and Buch in their studies of water heximer [35].

4.2. *Adiabatic DMC*

An approach that we developed to circumvent the challenges of obtaining a representation of $|\Psi|^2$ is called adiabatic diffusion Monte Carlo, or ADMC. This method is based on the finite field approach that has been applied in a variety of contexts where wave functions are not readily available. It was first applied to DMC by Sandler *et al.* [78]. The basic idea is relatively simple [69, 79]. As was mentioned above, DMC provides an accurate method for finding the ground state energy of an arbitrary system. One can imagine taking the Hamiltonian for the system of interest and perturbing it by adding a term that is proportional to the observable that one wants an expectation value of, $\hat{W}$

$$\hat{H} = \hat{H}^{(0)} + \lambda \hat{W} \tag{9}$$

For this purpose, $\hat{W}$ may be any operator and can be differential or multiplicative. The only constraint is that the kinetic energy operator remains separable so that the DMC methods, presented in the previous section, may be applied.

Based on the results of perturbation theory, we find that if the Hamiltonian has a perturbation that is proportional to λ, then the energy can be expressed as an expansion in λ,

$$E_0 = E_0^{(0)} + \lambda E_0^{(1)} + \frac{\lambda^2}{2} E_0^{(2)} + \cdots \tag{10}$$

The term that is proportional to λ,

$$E_0^{(1)} = \left\langle \Psi_0^{(0)} | W | \Psi_0^{(0)} \right\rangle \tag{11}$$

is exactly the quantity of interest.

Within DMC, the procedure for solving this problem is a bit different than traditional perturbation theory. As is shown in figure 3, DMC provides the ZPE of the system as a function of τ. If we replace the Hamiltonian for the system, with the Hamiltonian in equation (9), and make λ a linear function of τ, $W(\tau)$ will no longer fluctuate around the ZPE, but instead will fluctuate about a low-order polynomial in τ or equivalently λ. This is illustrated in figure 4 for a simulation of $H_3O_2^-$ in which $\hat{W}$ is the OO distance, R_{OO}. For this simulation, $d\lambda/d\tau$ is chosen so that the change in the ZPE due to the perturbation is small compared to the statistical fluctuations of the simulation. In this sense, the perturbation is introduced *adiabatically*.

The advantage of this approach is that it provides a method by which the determination of the averages has the same accuracy as the DMC energy simulations. The disadvantage is that separate simulations must be run for each property of interest.

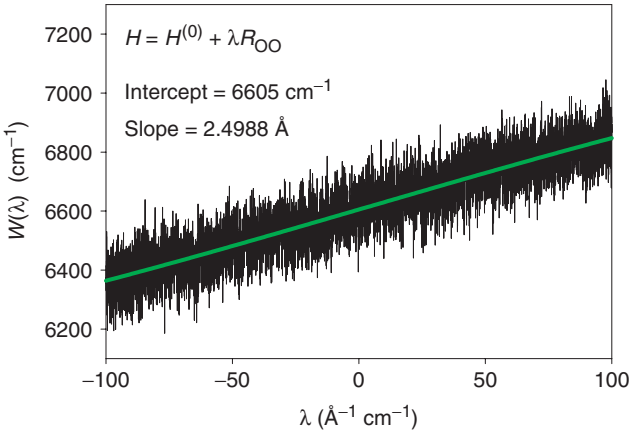

Figure 4. Sample plot of the results of an ADMC simulation of $\langle R_{OO} \rangle$ for $H_3O_2^-$.

In the more recent studies, we have abandoned this approach in favor of the descendent weighting (DW) method, described next.

4.3. *Descendent weighting*

A third option, and one that we have adopted for most of the work presented here, is the approach of DW [65]. This is also closely related to the idea of forward/backward counting of Rothstein [80]. The philosophy is based on the fact that calculating $|\Psi|^2$ at a particular configuration requires the evaluation of the wave function at that point by two different methods. As mentioned before, the distribution of the positions of the walkers at time τ provides a Monte Carlo sampling of the wave function at that time. Evaluating $|\Psi|^2$ requires a method to evaluate the magnitude of the wave function at the position of each of the walkers. One way to determine this is to count the number of descendants a particular walker has after a specified number of time-steps. It is easy to see why this procedure should provide the desired information. If the walker is in a classically allowed region of the potential, for example, near the potential minimum, the walker will span numerous progeny and these new walkers will, in turn, generate additional walkers. This leads to a relatively large weight associated with this walker. On the other hand, a walker that is in a classically forbidden region has less probability for spawning progeny and there is a reasonable probability that it will be removed from the simulation. As with a continuous weighting scheme, care must be taken with the number of time-steps over which the descendants are counted. If the time is too little then all the walkers will have equal probability. If too long a time is used then most of the original walkers will have been annihilated.

The DW approach has the additional advantage over the ADMC approach that one can use the resulting $|\Psi|^2$ to obtain projections of the probability amplitude onto any single internal coordinate, or, for that matter any subset of internal coordinates. This can be useful if one is interested in obtaining the probability amplitude associated with a vibrational motion in these molecular clusters or ions. A comparison of results of the DW and AVPC approaches can be found in table 1 of reference [77].

4.4. *Example 1 – Bond lengths in $H_3O_2^-$*

To illustrate the aforesaid three approaches, we have computed the average values of the OO and OH distances for $H_3O_2^-$ by the AVPC and DW approaches, described previously. Comparing the values in table 2 to the slope in figure 4 we find that the agreement among the three approaches is quite good. As, of the three, the DW approach is the most efficient; it is the one that we have used in most of our recent applications of DMC.

4.5. *Example 2 – Bond length distributions for CH_5^+ and CD_5^+*

As noted already, CH_5^+ presents a particularly interesting case study for DMC due to the equivalence of the five hydrogen atoms. This leads to a lack of a single reference structure for basis-set approaches. The reason for this is illustrated in figure 5.

Table 2. Averages of various distances in $H_3O_2^-$, evaluated by DW and AVPC.

Quantity	DW	AVPC
R_{OO}	2.497 Å	2.501 Å
r_{OH} [a]	0.981	0.980
r_{OH} [b]	1.267	1.263

[a] Outer OH distance.
[b] Inner OH distance.

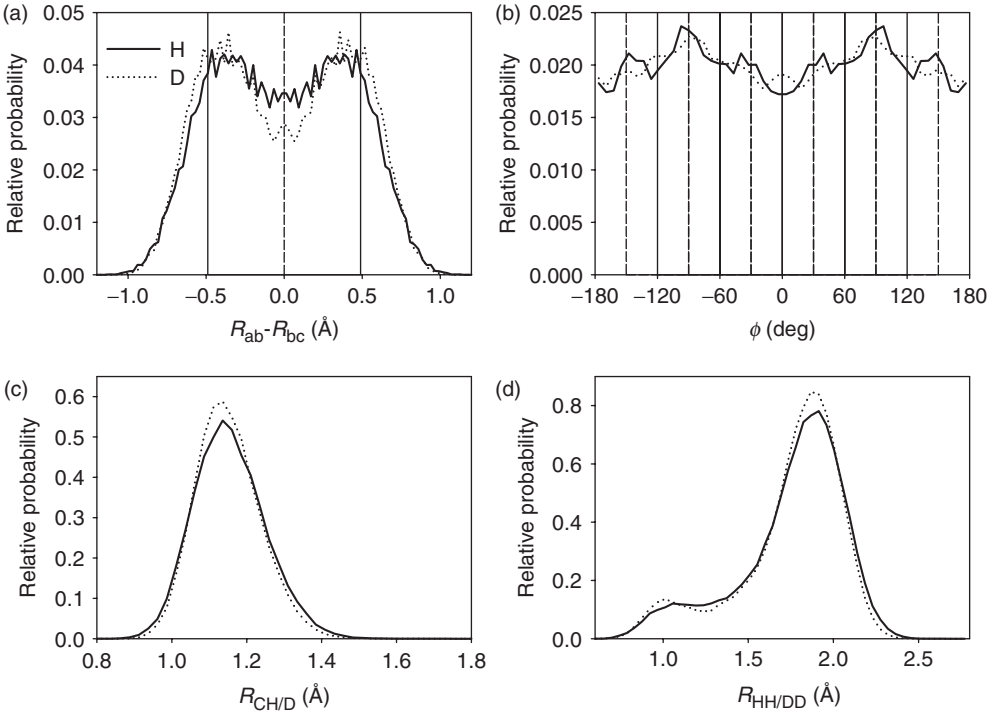

Figure 5. The probability distributions for the ground state of CH_5^+ (solid line) and CD_5^+ (dotted line), plotted as a function of the two isomerization coordinates, the CH and HH distances. In (a) and (b) vertical solid lines represent the values of the coordinate at the equilibrium configurations, dashed lines give the value of the coordinate at the corresponding first-order saddle point.

Here, we plot the probability amplitude for the ground state of CH_5^+, projected onto the two coordinates that correspond to motion from the C_s(I) global minimum toward the two saddle-point structures, plotted in figure 2(c). In figure 5(a), we project $|\Psi|^2$ onto ϕ, the coordinate that corresponds to rotation of the CH_3^+ subunit off the plane contains the carbon atom and the hydrogen atoms that are labeled a and b in figure 2(c). For these plots, $\phi = 0$, ± 60, and ± 120 correspond to the minimum energy configurations, whereas $\phi = \pm 30$, ± 90, or ± 150 correspond to the C_s(II) saddle-point geometries. As is seen, the probability amplitude is roughly equal at all values of ϕ, and, if anything, is

somewhat larger at the saddle-point than at the minimum. Similar behavior is seen in classical trajectories for this system [57]. We believe this behavior reflects the fact that, when ZPE is taken into account, the lower energy configuration is, in fact, the C_s(II) saddle-point structure. This is supported by the fact that on an earlier version of the potential used in the present work, evaluated at the same geometries but using MP2 level calculations to generate the electronic energies [56, 57], we found that when tritium was substituted for hydrogen, the probability amplitude at the C_s(I) minimum increased relative to that at the C_s(II) saddle-point. Independent of small fluctuations, we find that there is nearly equal amplitude as the CH_3^+ unit is rotated.

The second low-energy saddle point corresponds to a flipping motion of H_b between H_a and H_c. We can characterize this motion by plotting the probability amplitude as a function of the difference between the $H_a - H_b$ distance and the $H_b - H_c$ distance. This is plotted in figure 5(b). As is seen, the amplitude is larger near the C_s(I) minimum energy configuration, depicted by vertical solid lines, although the maxima occur at slightly shorter distances. In addition, there is significant probability amplitude when the two HH distances are equal, e.g. near the C_{2v} saddle-point. Deuteration will spread out the distribution and decrease the amplitude at the C_{2v} saddle-point structure, but the amplitude still remains significant. These results serve to illustrate that the wave function is completely delocalized over both of the low-lying barriers for isomerization, even in the ground vibrational state. When we plot the probability distributions as functions of the HH or CH distances for each possible combination of H atoms they are found to be identical, as seen in panels (c) and (d) of figure 5. This is in spite of the fact that the initial conditions for the simulation are based on a single minimum energy geometry. This further serves to illustrate that the DMC simulation does allow the walkers to sample all energetically accessible minima when there is probability amplitude in the tunneling region. In cases where the barriers are high and the amplitude at the tunneling region is nearly zero, such an exchange will not take place. Examples of this include the exchange of the central and outer hydrogen atoms in $H_3O_2^-$ or $H_5O_2^+$.

4.6. *Example 3 – Rotational constants*

Important properties, as we consider interpreting spectra, are the rotational constants. These quantities are tricky as they are not cleanly associated with specific operators. Instead, they result from applying second-order perturbation theory to the full rotation-vibration Hamiltonian, and, experimentally, arise from fitting a series of ro-vibrational transitions to a model Hamiltonian. As such, one way to obtain these quantities would involve evaluating rotationally excited states by DMC – something that has been pursued by Whaley *et al.* [81, 82].

An alternative is to construct an approximate operator for the rotational constants. Since the rotational constants are proportional to the elements of the inverse of the moment of inertial tensor, one way to evaluate them by DMC is to average the six unique elements of this matrix over the probability amplitude, obtained by DMC. In the case of relatively rigid complexes, a geometrical embedding can be employed. This is the approach we took for our studies on Ne_nSH and Ne_nOH. In these systems,

Table 3. Rotational constants for Ne_nOH.

n	Calculation	A/MHz[a]	B/MHz	C/MHz
2	Equilibrium[b]	6022.5	5672.7	2921.2
	Eckart[c]	5183 (45)	5114 (53)	2436 (19)
	Geometric[d]	5159 (33)	4981 (31)	2459 (33)
	Eckart[e]	5322 (63)	5140 (39)	2458 (17)
3	Equilibrium	2902.4	2783.8	2783.8
	Eckart	2403 (11)	2375 (25)	2360 (17)
	Geometric	2454 (23)	2398 (29)	2392 (26)
4	Equilibrium	2797.5	1492.1	1492.1
	Eckart	1916 (23)	1657 (43)	1055 (27)

[a] One standard deviation based on 5 ADMC calculations.
[b] Value of the constants evaluated at that stationary point.
[c] Value of the vibrationally averaged constants using an Eckart embedding.
[d] Value of the vibrationally averaged constants using a geometric embedding.
[e] Ne_2OD.

the z-axis is chosen to be the vector that connects the centers of mass of O/SH to the center of mass of the neon atoms, while the neon complex is chosen to be symmetric with respect to reflection in the yz-plane, when the complex is in its minimum energy configuration. Here the rotational constants are represented by the average values of the diagonal elements of the inverse of the moment of inertia tensor. The results for Ne_nOH ($n = 2$–4) are given in table 3 .

A second possible choice is to employ an Eckart embedding of the body-fixed axis system [83]. We are not the only group to take this approach. Buch and co-workers used an Eckart embedding in their studies on CO–H_2O [77] while Jordan and co-workers used it for their studies of CH_5^+ [62]. For this approach, we follow the work of Louck and Galbraith [84]. The first step is to define a static molecular model, which is typically a stationary point on the potential. For this static molecular model, the positions of the N atoms are described in Cartesian coordinates, and the origin is at the center of the mass. The position of the ith atom is represented by $\mathbf{a}^{(i)}$. At any arbitrary configuration, the coordinates of each of the atoms are given by $\mathbf{r}^{(i)}$ and the Eckart vectors are given by

$$\mathbf{F}_\alpha = \sum_{i=1}^{n} m^{(i)} \mathbf{a}_\alpha^{(i)} \mathbf{r}^{(i)} \tag{12}$$

where α represents one of the Cartesian coordinates and $m^{(i)}$ is the mass of the ith atom. Recalling that in the Eckart frame, the goal is to minimize the so-called *vibrational angular momentum*, the three unit vectors that define the Eckart frame are given by

$$\left[\hat{f}_x,\ \hat{f}_y,\ \hat{f}_z\right] = \left[\mathbf{F}_x,\ \mathbf{F}_y,\ \mathbf{F}_z\right] F^{-1/2} \tag{13}$$

Table 4. Rotational constants for CH_5^+.

Reference	Calculation	A/cm^{-1} [a]	B/cm^{-1}	C/cm^{-1}
C_s(I)	Equilibrium[b]	4.441	3.842	3.644
	Eckart[c]	3.906 (0.017)	3.860 (0.025)	3.836 (0.025)
C_{2v}	Equilibrium	4.376	3.961	3.779
	Eckart	3.910 (0.019)	3.855 (0.026)	3.838 (0.020)
C_s(II)	Equilibrium	4.443	3.822	3.645
	Eckart	3.903 (0.025)	3.862 (0.032)	3.838 (0.021)

[a] One standard deviation based on 16 calculations of the probability amplitude.
[b] Value of the constants evaluated at that stationary point.
[c] Value of the vibrationally averaged constants using an Eckart embedding.

In this approach, for each of the walkers, the inverse of the moment of inertial tensor is evaluated in the Eckart frame and the matrix elements are averaged over the ensemble (or evaluated by ADMC, in the case of Ne_nOH). Comparison between the above two approaches for Ne_nOH is given in table 3. In most of the cases, the average rotational constants are much smaller than the corresponding values at the stationary points that are within $10\,cm^{-1}$ of the global minimum. On the other hand, both the approaches yield rotational constants that agree within twice the standard deviations of the calculations. Where there are differences, these can easily be rationalized [71].

While the Ne_nOH systems are relatively floppy, the facts that the rotational constants are determined by the masses of the heavy atoms, and the positions of the heavy atoms remain close to their minimum energy configuration in the ground vibrational state make the evaluation of the rotational constants relatively insensitive to the choice of embedding. This will not be the case for molecules like CH_5^+ for which the carbon atom is near the center of mass of the ion and the rotational constants are affected by the large amplitude motions of the hydrogen atoms. In fact, attempts to use a geometrical embedding for this system will yield unphysical results. Instead, we employ an Eckart embedding, based on each of the three low-energy stationary points on the potential surface, shown in figure 2(c). At first glance, it is not clear that an Eckart embedding should be appropriate for this system. In table 4, we report the rotational constants at the three stationary points as well as those obtained by an Eckart embedding that employs each of them for its static molecular model. As is seen, the differences among the static rotational constants are large, but the vibrationally averaged ones agree to within the statistical uncertainties. Further, the three rotational constants are nearly equal. For comparison, Jordan and co-workers report vibrationally averaged rotational constants of 3.83, 3.80, and $3.78\,cm^{-1}$ using their potential surface and we predicted an average value of $3.91\,cm^{-1}$ from the fit MP2 surface of Brown *et al.* [57]. The DMC rotational constants, reported above, have been used by Savage and Nesbitt to assign a band origin at $2950\,cm^{-1}$ in their rotationally resolved spectrum for CH_5^+ [19].

For $H_5O_2^+$ and $H_3O_2^-$, the difference between the masses of the hydrogen and oxygen atoms makes them very close to symmetric top molecules. For example, the

vibrationally averaged rotational constants for $H_3O_2^-$ are 10.2497, 0.308, and 0.305 cm^{-1}, while for $D_3O_2^-$, they are 5.5028, 0.282, and 0.279 cm^{-1} and the corresponding κ values are -0.9994 and -0.9989 [85]. This contrasts the values at the linear saddle-point, the lowest energy stationary point shown in figure 2(a) when ZPE is taken into account, of 10.2651, 0.3213, and 0.3196 cm^{-1} for $H_3O_2^-$ and 5.5067, 0.2933, and 0.2908 cm^{-1} for $D_3O_2^-$. The similarity of the B and C constants for this system is not surprising as most of the mass is on the two oxygen atoms and it is their distance that, to the lowest order, determines these constants. The large increase, 5% for $H_3O_2^-$ and 10% for $D_3O_2^-$ reflects the relatively larger amplitude excursions the three hydrogen atoms off the OO bond axis.

We have also evaluated the vibrationally averaged rotational constants for $H_5O_2^+$. As with $H_3O_2^-$, $H_5O_2^+$ is nearly a symmetric top, the constants, evaluated at the potential minimum are 5.8520, 0.2915 and 0.2903 cm^{-1} for $H_5O_2^+$ and 2.9828, 0.2405, and 0.2387 cm^{-1} for $D_5O_2^+$. When zero-point motions are considered, the vibrationally averaged constants are 5.776, 0.2804, and 0.2803 cm^{-1} for $H_5O_2^+$ and 2.9545, 0.2318, and 0.2316 for $D_5O_2^+$, and corresponding κ values are -0.99996, and -0.99985, when the equilibrium geometry is used for the static molecular model. Using the C_s or C_{2h}, *trans*, saddle point configurations gives constants that differ by less than 0.04%. On the other hand, if the C_{2v}, *cis*, saddle-point is used for the static molecular structure, the averaged constants are very different, reflecting the fact that there is very little amplitude near this configuration.

5. Excited states

One of the long-standing challenges with the DMC approach arises from the fact that it is fundamentally a ground state method. In order for it to be a useful tool for investigating systems of chemical interest, one needs to have a way to handle states that contain nodes. For electronic structure problems, nodes must be considered even about the ground state. For vibrational problems, in order to obtain information for states besides the ground state, nodes must be included in the calculation. A number of methods for evaluating vibrationally excited states have been considered. Coker and Watts introduced a method based on the orthogonalization of wave functions [87]. Ceperley and Bernu have developed a correlation function based approach for obtaining the energies of excited states [87]. This approach was applied to the $H_5O_2^+$ system by Cho and Singer [48], using their OSS3(p) potential surface [46]. Whaley and co-workers have used a related approach, termed POITSE [81], to evaluate rotational excited states of molecules in helium droplets. In what follows, the focus is on an alternative approach, based on the *fixed-node* approximation [64].

Specifically, in a case where the functional form of an $n-1$-dimensional nodal surface is known, for example by symmetry, evaluation of an excited state wave function and energy is straightforward. Mathematically, in the region of a node a wave function behaves in exactly the same manner as it would if the potential had been made infinite along the nodal surface. Specifically, the wave function goes to zero at the node, while the first derivative is finite. This can most easily be seen in one dimension. For example, consider the Morse oscillator potential, shown in figure 6(b).

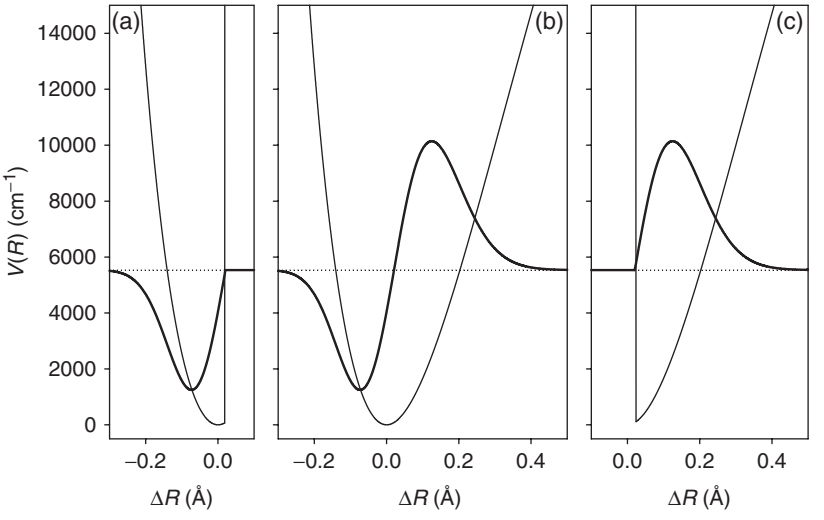

Figure 6. Plots of three potentials and their corresponding wave functions, all of which have the same energies. The central plot shows a Morse oscillator with parameters to model an OH stretch, along with the wave function for the first vibrationally excited state. On the left and right, the potential is replaced by an infinite potential at the value of R at which the wave function in (b) has a node. The resulting ground state wave functions are superimposed on the potentials, plotted in (a) and (c).

The energy of the state with $n = 1$ is the same as the energies of the ground states of the potentials, plotted in panels (a) and (c). In addition, the corresponding wave function, plotted in (b) is the sum of the wave functions plotted in the other two panels.

As the plots in figure 6 show, when we know where the node(s) should be placed, excited state calculations can be reduced to a series of ground state calculations in which infinite potentials are introduced at the nodes, effectively dividing the surface into a series of regions over which the wave function does not change sign. Such a series of ground state calculations can be evaluated readily by using DMC. Nearly 30 years ago, Anderson provided a simple algorithm for calculating excited state wave functions within this *fixed node* approach. As wave functions cannot penetrate infinite potential barriers, any walker that crosses the nodal surface must be removed from the simulation. In the limit of infinitely short time-steps, this condition is sufficient to ensure that the excited states are properly described. For finite time-steps, the possibility that a walker crosses the nodal surface twice, starting and ending on the same side of the node, must be accounted for. This is accomplished by introducing a *recrossing correction* that introduces the probability that a walker that remains on the same side of the nodal surface before and after a time-step has actually crossed the node twice [64].

The above procedure is arguably the most effective approach for introducing nodes into DMC simulations, but it requires *a priori* knowledge of the functional form of the nodal surface. This is perhaps the greatest obstacle for applying DMC to electronic structure problems. For vibrational systems, the problems are more or less severe, depending on one's perspective. The challenges in vibrational problems come from

the larger density of states. As a result, multiple vibrational states are typically of interest, whereas there are many interesting systems where the chemistry takes place on a single electronic state. On the other hand, in contrast to electronic structure problems, the ground vibrational state is nodeless. Drawing on the expectation that, to lowest order, the vibrations in a N-atomic system can be described as $3N-6$ uncoupled oscillators (which may or may not be harmonic), one expects that the nodal surfaces can be approximated by a function of a single vibrational coordinate. In other words, the wave function that corresponds to a state with one quantum of excitation in mode j will change sign when $q_j = \eta_j$. This treatment is the basis of a normal mode picture of molecular vibrations, which can easily be shown to be valid in the limit of small amplitude displacements from a single minimum energy structure. For these floppy systems, such a treatment is clearly oversimplified, and has led some people to conclude that the fixed-node approach will be futile for systems as floppy as $H_5O_2^+$ [48], but, as can be seen, at the level of the fundamentals, careful choice of these vibrational coordinates can lead to a good approximation to most, if not all, of the states with one quantum of excitation.

While the above lays the groundwork for obtaining excited states, a significant issue remains. That is, determining the value of η_j at which the wave function is expected to change sign. In some cases symmetry considerations may be used to define the position of the nodal surface. In many cases, this is not possible. One alternative is to follow an approach commonly taken in electronic structure calculations and use nodes from wave function that are obtained by an approximate approach. This possibility was explored by Gerber and co-workers, where they used the excited state wave functions, obtained from vibrational self-consistent field (VSCF) calculations to obtain excited state energies for Ar_3 and Ar_{13} [88].

Before addressing how we determine the value of η_j in these cases, it is useful to consider the various relationships among the properties of the three wave functions plotted in figure 6. These ideas were originally described by Buch and co-workers [78]. First, the energies associated with the three wave functions are identical. In addition, the first derivative of the wave functions plotted in (a) and (c) are the same at the point they go to zero. If the position of the node were moved to the right, the energy of the state that is localized on the left side of the node would decrease, while the one on the right side would increase due to quantum mechanical effects of confinement.

Severson and Buch used the above considerations to find the energies of the fundamentals of $(H_2O)_6$. In that study, they used trial-and-error to locate the optimal positions of the nodal surfaces [35]. The challenge of that approach comes from the fact that the energies evaluated by DMC contain statistical uncertainties. Therefore, matching energies of individual simulations is numerically challenging. To address this, we have applied the above considerations to determine the optimal value of η_j, within the context of an ADMC simulation [69, 79]. As in the evaluations of expectation values by ADMC, we slowly vary the Hamiltonian that is being solved during the simulation. In this case, the parameter that is being varied is the position of the nodal surface for a fixed-node calculation. In this approach, two simulations must be run, one for each of the two parts of the wave function, shown in figure 6(a) and (c). The resulting energies are plotted as functions of the position of the nodal surface,

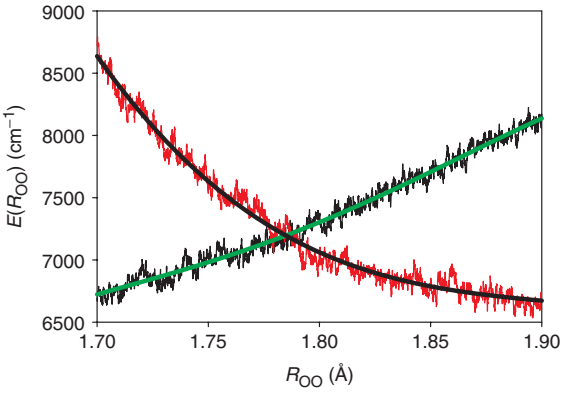

Figure 7. Plots of the energy as a function of the position of the nodal surface. In this case, the node is chosen to be along the OO stretch in $H_3O_2^-$. As is seen, the two curves form a cross, and fitting them to low-order polynomials allows us to identify the energy of the first excited state as well as the position of the node.

and the point at which these two curves cross provides the position of the node and the corresponding energy. Due to the numerical noise associated with DMC simulations, we find that this is most easily accomplished by fitting the plots of $W(\eta)$ to a low-order polynomial expansion in η, prior to finding the crossing point. The results of a typical simulation are shown in figure 7, where we calculated the energy of the fundamental in the OO stretch in $H_3O_2^-$.

5.1. *Example 4 – The stretch fundamental in Ar_3*

As an initial test of this approach, we repeated the fixed-node calculations of Broude and Gerber on the argon trimer system. In this system, the three vibrational modes are divided into a doubly degenerate bend and a symmetric stretch. As such, the node for the bend-fundamental can be determined by symmetry, whereas an approach for locating the node is needed to obtain the fundamental in the symmetric stretch. Our ADMC calculation predicts this energy to be at 74.66 cm^{-1}, while the fixed-node calculations for this system, in which the nodes were determined by the VSCF wave function gives an energy of 76.76 cm^{-1} [88]. Converged variational calculations of Cooper, Jain, and Hutson using the same potential predict an energy of 74.37 cm^{-1} [89]. The fact that the ADMC energy is closer to the variational result than the DQMC/VSCF is not entirely surprising as VSCF is a variational procedure that will yield the separable wave function optimized to minimize the energy. It has been shown that alternative procedures, for example, a natural modal analysis that optimizes the overlap, between a separable wave function and the true ground state wave function, will yield different solutions [90]. What is somewhat more surprising is the level of agreement between the fixed-node ADMC energy and the variationally optimized energy for the same system. For weakly bound systems, one might expect that, even at the fundamentals, the wave function is highly anharmonic and not separable. We will return to this point in our discussion of the second set of systems.

5.2. *Example 5 – The fundamentals in Ne_2XH*

To further test the ADMC approach, we calculated the six fundamentals of Ne_2OH and Ne_2SH. The results are reported in table 5. As in Ar_3, these clusters are anticipated to undergo large amplitude motions, even in their ground vibrational states. This is illustrated in the projections of the probability amplitudes onto the two Ne–OH stretch and bend coordinates, shown in figure 8(a) and (b). The amplitude is particulary large in the in-plane bend coordinate which corresponds roughly to OH rotation in the plane of the complex. The analogous plots for Ne_2SH look nearly identical although the amplitude of the motion is larger for the OH complex than for the SH one. This reflects the fact that the Ne–SH potential is more isotropic than the one for Ne–OH [43, 44]. In fact, examination of the Ne–OH potential shows that it more closely resembles that of a bound triatomic molecule than a typical van der Waals system. This leads to greater localization of the OH in a near-linear Ne–OH configuration in the dimer, but when a second neon atom is introduced, this also leads to a larger amplitude in-plane OH motion, compared to the Ne_2SH complex.

Examination of table 5 shows that, in general, the ADMC energies of the fundamentals are in very good agreement with those obtained by converged variational calculations. Exceptions are found for the in-plane bend for Ne_2OH and for the Ne–XH symmetric stretch in both complexes. We shall return to these later. For the remaining states, the differences are in the order of 0.5–1.0 cm^{-1}. This agreement is excellent given the fact that the nodal surfaces are assumed to be functions of a single internal coordinate, or symmetry adapted linear combinations of internal coordinates that reflect the fact that these complexes have C_{2v} symmetry in their equilibrium configurations.

The agreement may, at first, be surprising given that these are rather floppy systems. We believe, it reflects the fact that while the simplicity of the functional form of the nodal surface could provide a strong constraint on the description of the system, we have optimized the wave function within this constraint. Specifically, there are not any constraints on the extent of the motion in the other degrees of freedom, and, for example, if we look at the fundamental in the Ne_2–OH stretch, we find that as the Ne_2–OH distance is increased, the amplitude of the OH bending motion also

Table 5. Comparison of DMC and var energies for low-lying vibrational states in the T-shaped minimum of the Ne_2XH potential.

	Ne_2SH		Ne_2OH	
State	DMC[a]	var	DMC	var
Ground state	−102.4	−102.3	−112.4	−112.2
Ne–XH–Ne bend	17.1	17.3	18.2	17.8
Ne_2 bend	19.2	19.3	22.1	20.8
Ne_2–HX stretch	23.3	25.4	33.5	28.4
In-plane bend	33.4	32.9	[b]	[b]
Out-of-plane bend	40.8	40.8	77.6	78.5

[a] All energies are reported in cm^{-1}. The ground state energy is reported relative to the Ne + Ne + XH dissociation limit while all other energies are reported relative to the ground state energy.
[b] The in-plane bend fundamental does not exist in Ne_2OH.

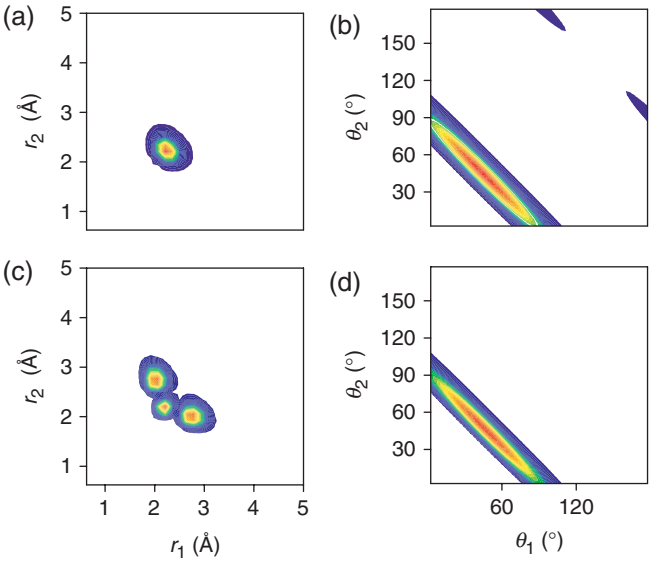

Figure 8. Projections of the wave functions for $Ne_2(OH)$ along the two Ne–OH distances, r_1 and r_2 and slices through the wave function in the two Ne–OH angles. These wave functions were obtained from the variational calculations, described in [45]. Plots for the ground state are shown in (a) and (b), while (c) and (d) give results for the fundamental in the Ne–OH symmetric stretch.

increases, compared to that seen in the ground state. Conversely, as the Ne_2–OH distance decreases, the amplitude of the bending motion is decreased [71]. In addition, we know that in the limit of very small amplitude motions, the vibrational wave function is separable. In these more fluxional systems, one expects that anharmonicity will become more important, but in the absence of near resonances, there is no reason to expect that the nodal surfaces that are needed to obtain the fundamentals will be complicated functions of the internal coordinates, assuming that these coordinates are picked carefully.

A notable exception to this good agreement is seen in the Ne–XH symmetric stretch in both Ne_2SH and Ne_2OH. The reason for this can be understood by an examination of the projections of the wave function, obtained by the variational calculations for this state in Ne_2OH and plotted in figure 8(c) and (d). For this state, the node has distinct curvature in the r_1/r_2 plane, while the DMC simulations assumed that the node can be described by $r_1 + r_2 = \eta$. This was not considered in the DMC simulations which were performed several years prior to the variational calculations [45, 69, 71]. More recent work on $H_3O_2^-$ and HOOH has allowed us to investigate ways to handle this curvature and to identify when it is a concern. A more complete discussion of these issues can be found elsewhere [27].

In the case of the in-plane bend fundamental in Ne_2OH, the relatively large amplitude motion of the in-plane bend, even in the ground state and the relatively low energy conformer with a linear Ne–OH–Ne geometry made the lowest energy state with a node in this coordinate correspond to the ground state of the

Ne–OH–Ne conformer. In fact, this simulation yields an energy of 34.56 cm^{-1}, which is in good agreement with the energy of the lowest energy state in the linear Ne–OH–Ne minimum with the same symmetry, 34.51 cm^{-1}.

5.3. *Example 6 – Fundamental vibrations in $H_3O_2^-$ and $D_3O_2^-$*

A third set of systems for which we have made comparisons with variational results for all of the fundamentals is $H_3O_2^-$ and $D_3O_2^-$. In contrast to the two systems, described above, the fact that these ions contain five atoms means that they are beyond the size of species for which variational calculations can be performed and converged to better than 0.1 cm^{-1} accuracies that were reported for Ar_3 and Ne_2XH. As such, for these systems we draw from our experience with the rare gas complexes as well as trial studies on closely related systems, HOOH and H_3O^+, for which comparisons to converged and fully converged calculations can be made. Based on that work, we expect that the excited state energies, obtained from the DMC simulations should, for the most part, provide semi-quantitative descriptions of these states.

In table 6 we report the energies for $H_3O_2^-$, obtained by ADMC and using MULTIMODE [27]. Details of both the calculations can be found elsewhere. The important point is that the two sets of calculations are in overall good agreement. For states with energies below 600 cm^{-1}, the differences for $H_3O_2^-$ are less than 15 cm^{-1}, and the splitting between the + and − states are also in good agreement. For this system, the difference between the + and − states is the introduction of nodes at the

Table 6. Energies of the fundamentals of $H_3O_2^-$ and $D_3O_2^-$ obtained from DMC and VCI[a] calculations.

	$H_3O_2^-$				$D_3O_2^-$			
	VCI		DMC[b]		VCI		DMC	
Mode	+[c]	−	+	−	+	−	+	−
Ground[d]	6625	22	6605	14	4882	6	4877	4
Torsion	132	215	131	224	108	143	103	145
OO stretch	515	540	505	521	493	509	491	495
Wag	576	606	588	602	398	406	437	437
Rock	465	528	479	517	319	349	354	368
z	741	785	644	665	484	512	402	408
x	1299	1426	1102	1110	982	1020	792	797
y	1473[e]	1518	[f]	1019	1094	1100	[f]	713
OH-sym[g]	3641	3666	3631	3641	2681	2689	2678	2682
OH-asym[g]	3634	3666	3609	3625	2681	2699	2664	2667
OH-local			3610	3632			2668	2673

[a] The details of the VCI calculations are given in [27].
[b] All DMC results contain a 5 cm^{-1} statistical uncertainty.
[c] The + and − states represent the lower and upper states of the tunneling doublets.
[d] The ground state energy is reported relative to the potential minimum. All other energies are reported relative to the ground state.
[e] Several states between 1320 and 1618 cm^{-1} contain significant character of this fundamental.
[f] This state could not be identified from the fixed-node DMC calculations.
[g] For these states there is at least one other state with significant OH or OD stretch character within 10 cm^{-1} (OH) or 3 cm^{-1} (OD) of the reported energy.

cis- and *trans*-configurations of the HOOH group for the − state, while it is nodeless in the + state.

As noted above, for $D_3O_2^-$, the DMC and MULTIMODE ZPEs differ by only $5\,cm^{-1}$, which is roughly the statistical uncertainty of the DMC simulation. On the other hand, the difference in the frequencies of the four lowest frequency modes are larger for $D_3O_2^-$ than for $H_3O_2^-$. One likely reason for this is that deuteration will make $D_3O_2^-$ more normal mode-like. This will help to make the MULTIMODE calculations, that are based on a normal mode basis, more accurate, while it will also mean that the nodes are less well described by functions of symmetry adapted linear combinations of the internal coordinates. The latter factor will render the ADMC results somewhat less accurate.

The next three states in the list correspond to Cartesian displacements of the central hydrogen atom. For these states, the fundamentals in the *z*-displacements of the central hydrogen atom are in fairly good agreement, but given the large amplitude of this motion, it is a challenge for both the approaches. The perpendicular displacements are more challenging. Here, the difficulty reflects the fact that there is a significant coupling between these modes and the wag and rock mode of the outer hydrogen atom. More recent calculations show that placement of the nodes along the coordinates that are linear combinations of these four modes yields, energies that are closer to those obtained from the MULTIMODE calculations.

The last two states are the stretches of the outer hydrogen atoms. If we take a *normal mode* approach, we find that these two states are slit by roughly $20\,cm^{-1}$ in $H_3O_2^-$ and by $14\,cm^{-1}$ in $D_3O_2^-$. If, on the other hand, we localize the excitation, we find that the energy is very close to the asymmetric stretch energy, in all the cases. Based on what we found for the Ne_2XH systems, we believe that the localized OH stretch provides a more faithful representation of the nodal surface in these cases.

6. Using DMC to interpret spectra

One of the exciting and interesting aspects of the systems that we have used to illustrate DMC approaches comes in the fact that all of them are of experimental interest. For nearly all of these systems, spectra have been reported, but not fully assigned. The reason we initially began investigating DMC was to provide inputs that might aid in the assignment of the electronic spectrum of Ne_2OH that had been measured by Miller and co-workers [91]. While having the ability to evaluate probability amplitudes, vibrationally averaged rotational constants and approximations to the anharmonic vibrational frequencies, through the fixed node approximation are all useful, to make full comparisons, one needs to be able to evaluate the intensity as well as the position of the transitions.

For $H_3O_2^-$ and $H_5O_2^+$, we have employed the AVPC approach [78]. In contrast to the systems investigated with this approach by Buch and co-workers, both $H_3O_2^-$ and $H_5O_2^+$ are essentially symmetric tops, having $\kappa < -0.999$. This leads to difficulties in embedding the body-fixed axis system for these species. In spite of this, we have computed the intensities for a variety of transitions of these complexes and find that they are in good agreement with those obtained from MULTIMODE [74].

As mentioned above, this approach can be tedious and it seems that, at least for the interpretation of low to moderate resolution spectra, one should be able to find an easier way to achieve this. Work in this direction is currently underway.

In the case of CH_5^+, we have taken a somewhat different approach for obtaining information about the spectra in the CH stretch and HCH bend regions of the spectrum for which a laser induced reaction (LIR) spectrum has recently been reported [9]. Although somewhat surprising at first, in many cases the scaled harmonic calculations provide very good approximations to both the positions and intensities of the lines associated with intramolecular vibrations in hydrogen bonded clusters. Given that CH_5^+ samples multiple minima and the connecting saddle points even at the zero-point level, such a simple approach is not advisable here. On the other hand, we have had good success calculating the spectra of CH_5^+ using either variational (e.g. MULTIMODE) or harmonic calculations that are based on a single reference geometry and weighting them by the probability amplitudes at those geometries, obtained from DMC calculations. While this approach cannot provide an accurate high resolution spectrum, it reproduces the major features in the CH stretch region down to a $10\,cm^{-1}$ resolution [19].

7. Summary and future prospects

In this review, we have summarized some recent advances in DMC as it is applied to molecular clusters and molecular ions. While significant progress has been made over the past decade and through this interesting insights have been gained into the spectroscopy and dynamics of the Ne_nXH, $H_3O_2^-$, $H_5O_2^+$ and CH_5^+ systems, issues remain to be addressed. Among these are: Can there be better ways to obtain intensities from the DMC simulations? Are there better or more systematic ways to select the coordinates for fixed-node calculations? What does one do when the system of interest cannot be described by a single adiabatic potential surface? Are there more efficient and more accurate ways that we can obtain excited states? Probably most important, the calculations described here all relied on having available a potential surface for the system of interest that could be evaluated at any energetically accessible configuration of the system. There are many systems of interest for which such potentials do not exist and can we find a way to work around these issues?

All of the above questions are being addressed either by us or by others. We are presently working to extend our approaches for spectral simulations for these systems. As rotationally resolved spectra become available [92], we also need to consider approaches for obtaining rotational information. Such work has been done for rotations of molecules within helium nano-droplets [81], but, in contrast to the systems considered here, these systems typically have a well-defined structure and are not as prone to the large Coriolis interactions as are seen in CH_5^+.

For non-adiabatic systems, we have been working on surface hopping approaches within DMC. An early account of these ideas is reported in [93], and preliminary work on the Ne_2OH $\tilde{X}$-state has been performed, in the hope to start deciphering the electronic spectrum for this complex.

The final question of potentials is also the most challenging one. We began this work looking at doped rare-gas clusters primarily because we could develop models for the potential surfaces as pair-wise sums of atom–atom or atom–molecule interactions. With time we have moved into other systems, but our choices of systems are limited by the availability of potential surfaces. While the calculations that are needed to evaluate the electronic energies of a system at a variety of points are well developed, taking this information and extracting a potential surface from it is much less so. In addition to Bowman and co-workers [50, 56, 57], with whom we have collaborated on much of the work described here, Jordan and co-workers have made good progress using DMC to choose points to perform electronic structure calculations and from that generate a potential by Shepherd interpolation techniques [94].

While considerable progress has been made in the applications of DMC approaches to studies of fluxional species, there are still a number of open issues and challenges. As computers and theoretical approaches that exploit advances in computer technology advance, larger and larger systems will be accessible by basis-set approaches, but as this happens, DMC should remain an attractive approach for exploring those systems that are at the edge of what is possible.

Acknowledgements

Support through grants from the Chemistry Division of the National Science Foundation as well as the Petroleum Research Fund, administered by the American Chemical Society, is gratefully acknowledged. The work at Ohio State would not have been possible without the efforts of Dr. John M. Herbert, Dr. Hee-Seung Lee, Benjamin M. Auer, and Lindsay M. Johnson. The author is also grateful to the experimental collaborators, Professors Terry A. Miller, Mark A. Johnson, and David J. Nesbitt, and their graduate students/post docs, Christopher C. Carter, Eric G. Diken, Jeffrey M. Headrick, and Chandra Savage, for numerous discussions and introducing us to some of the mysteries and challenges of the systems described here. Finally, the author thanks Professor Joel M. Bowman, Bastiaan J. Braams, Stuart Carter, and, in particular, Dr. Xinchuan Huang for allowing the author to utilize the potentials used in the studies of $H_3O_2^-$, $H_5O_2^+$ and CH_5^+, and for their many stimulating discussions and suggestions. Through this collaboration, the author has learned a lot about these systems as well as the capabilities and limitations of DMC.

References

[1] E. B. Wilson, J. C. Decius, and P. C. Cross, *Molecular Vibrations* (Dover, New York, 1955).
[2] H. H. Nielsen, Rev. Mod. Phys. **23,** 90 (1951).
[3] A. Thornley and J. M. Hutson, J. Chem. Phys. **101,** 5578 (1994).
[4] J. M. Hutson, J. Chem. Phys. **96,** 6752 (1992).
[5] S. S. Xantheas, J. Am. Chem. Soc. **117,** 10373 (1995).
[6] Y. Xie, R. B. Remington, and H. F. Schaefer III, J. Chem. Phys. **101**(6)**,** 4878 (1994).
[7] Z. Jin, B. J. Braams, and J. M. Bowman, J. Phys. Chem. A **110,** 1569 (2006).
[8] D. W. Boo and Y. T. Lee, J. Chem. Phys. **103**(2)**,** 520 (1995).

[9] O. Asvany, P. Kumar, B. Redlich, I. Hegeman, S. Schlemmer, and D. Marx, Science, **309,** 1219 (2005).
[10] L. I. Yeh, M. Okumura, J. D. Myers, J. M. Price, and Y. T. Lee, J. Chem. Phys. **91,** 7319 (1989).
[11] K. R. Asmis, N. L. Pivonka, G. Santambrogio, M. Bruemmer, C. Kaposta, D. M. Neumark, and L. Woeste, Science **299,** 1375 (2003).
[12] T. D. Fridgen, T. B. McMahon, L. MacAleese, J. Lemaire, and P. Maitre, J. Phys. Chem. A **108,** 9008 (2004).
[13] J. M. Headrick, J. C. Bopp, M. A. Johnson, J. Chem. Phys. **121**(23)**,** 11523 (2004).
[14] N. I. Hammer, E. G. Diken, J. R. Roscioli, E. M. Myshakin, K. D. Jordan, A. B. McCoy, X. Huang, S. Carter, J. M. Bowman, and M. A. Johnson, J. Chem. Phys. **123,** 044308 (2005).
[15] E. A. Price, W. H. Robertson, E. G. Diken, G. H. Weddle, and M. A. Johnson, Chem. Phys. Lett. **366,** 412 (2002).
[16] E. G. Diken, J. M. Headrick, J. R. Roscioli, J. C. Bopp, M. A. Johnson, A. B. McCoy, X. Huang, S. Carter, and J. M. Bowman, J. Phys. Chem. A **109,** 17 (2005).
[17] E. G. Diken, J. M. Headrick, J. R. Roscioli, J. C. Bopp, M. A. Johnson, and A. B. McCoy, J. Phys. Chem. A **109,** 1487 (2005).
[18] E. T. White, J. Tang, and T. Oka, Science **284,** 135 (1999).
[19] X. Huang, A. B. McCoy, J. M. Bowman, L. M. Johnson, C. Savage, F. Dong, and D. J. Nesbitt, Science **311,** 60 (2006).
[20] P. P. Kumar and D. Marx, Phys. Chem./Chem. Phys. **8**(5)**,** 573 (2006).
[21] H.-C. Chang, C.-C. Wu, and J.-L. Kuo, Int. Rev. in Phys. Chem. **24**(2–4)**,** 553 (2005).
[22] J. M. Bowman, S. Carter, and X. C. Huang, Int. Rev. Phys. Chem. **22,** 533 (2003).
[23] X. Huang, H. M. Cho, S. Carter, L. Ojamae, J. M. Bowman, and S. J. Singer, J. Phys. Chem. A **107,** 7142 (2003).
[24] J. Dai, Z. Bacic, X. C. Huang, S. Carter, and J. M. Bowman, J. Chem. Phys. **119,** 6571 (2003).
[25] X. Huang, B. J. Braams, S. Carter, and J. M. Bowman, J. Am. Chem. Soc. **126,** 5042 (2004).
[26] X. Huang, L. M. Johnson, J. M. Bowman, and A. B. McCoy, J. Am. Chem. Soc. **128,** 3478 (2006).
[27] A. B. McCoy, X. Huang, S. Carter, and J. M. Bowman, J. Chem. Phys. **123,** 064317 (2005).
[28] A. B. McCoy, X. Huang, S. Carter, M. Y. Landeweer, and J. M. Bowman, J. Chem. Phys. **122,** 061101 (2005).
[29] G. M. Chaban, J. O. Jung, and R. B. Gerber, J. Phys. Chem. A **104,** 2772 (2000).
[30] G. M. Chaban, S. S. Xantheas, and R. B. Gerber, J. Phys. Chem. A **107,** 4952 (2003).
[31] J. B. Anderson, Int. Rev. in Phys. Chem. **14,** 85 (1995).
[32] F. Paesani and K. B. Whaley, J. Chem. Phys. **121**(9)**,** 4180 (2004).
[33] D. F. Coker, R. E. Miller, and R. O. Watts, J. Chem. Phys. **82**(8)**,** 3554 (1985).
[34] D. F. Coker and R. O. Watts, J. Phys. Chem. **91,** 2513 (1987).
[35] M. W. Severson and V. Buch, J. Chem. Phys. **111,** 10866 (1999).
[36] M. Mella and D. C. Clary, J. Chem. Phys. **119,** 10048 (2003).
[37] A. Sarsa, Z. Bacic, J. W. Moskowitz, and K. E. Schmidt, Phys. Rev. Lett. **88,** 123401/1 (2002).
[38] W. A. Lester (Ed.), *Recent Advances in Quantum Monte Carlo Methods*, Recent Advances in Computational Chemistry (World Scientific, Singapore, 1997), Vol. 1.
[39] W. A. Lester, S. M. Rothstein, S. Tanaka (Eds), *Recent Advances in Quantum Monte Carlo Methods, Part II*, Recent Advances in Computational Chemistry (World Scientific, Singapore, 2002), Vol. 2.
[40] C. C. Carter, T. A. Miller, H.-S. Lee, and A. B. McCoy, J. Mol. Struct. **525,** 1 (2000).
[41] M. C. Heaven, Int. Rev. in Phys. Chem. **24**(3–4)**,** 375 (2006).
[42] R. A. Aziz and M. J. Salaman, Chem. Phys. **130,** 187 (1989).
[43] C. C. Carter, T. A. Miller, H.-S. Lee, A. B. McCoy, and E. F. Hayes, J. Chem. Phys. **110,** 5064 (1999).
[44] Lee, H.-S., A. B. McCoy, L. B. Harding, C. C. Carter, and T. A. Miller, J. Chem. Phys. **111,** 10053 (1999).
[45] H.-S. Lee and A. B. McCoy, J. Chem. Phys. **116,** 9677 (2002).
[46] L. Ojame, I. Shavitt, and S. J. Singer, Int. J. of Quant. Chem. **29,** 657 (1995).
[47] L. Ojame, I. Shavitt, and S. J. Singer, J. Chem. Phys. **109,** 5547 (1998).
[48] H. M. Cho and S. J. Singer, J. Phys. Chem. A **108,** 8691 (2004).
[49] J. P. Devlin, M. W. Severson, F. Mohamed, J. Sadlej, V. Buch, and M. Parrinello, Chem. Phys. Lett. **408,** 439 (2005).
[50] X. Huang, B. J. Braams, and J. M. Bowman, J. Chem. Phys. **122,** 044308 (2005).
[51] C. C. M. Samson and W. Klopper, J. Mol. Str. THEOCHEM **586,** 201 (2002).
[52] G. Zundel and H. Metzger, Z. Phys. Chem. (Munich) **58,** 225 (1968).
[53] D. J. Wales, J. Chem. Phys. **110,** 10403 (1999).
[54] E. Herbst, J. Phys. Chem. A **109,** 4017 (2005).
[55] A. Olah and G. Rasul, Acc. Chem. Res. **30,** 245 (1997).
[56] A. Brown, B. J. Braams, K. Christoffel, Z. Jin, and J. M. Bowman, J. Chem. Phys. **119,** 8790 (2003).
[57] A. Brown, A. B. McCoy, B. J. Braams, Z. Jin, and J. M. Bowman, J. Chem. Phys. **121,** 4105 (2004).

[58] H. Muller, W. Kutzelnigg, J. Noga, and W. Klopper, J. Chem. Phys. **106,** 1863 (1997).
[59] D. Marx and M. Parrinello, Science **284,** 59, 61 (1999).
[60] A. B. McCoy, A. Brown, B. J. Braams, X. Huang, Z. Jin, and J. M. Bowman, J. Phys. Chem. A **108,** 4991 (2004).
[61] L. M. Johnson and A. B. McCoy, J. Phys. Chem. A (submitted).
[62] K. C. Thompson, D. L. Crittenden, and M. J. T. Jordan, J. Am. Chem. Soc. **127,** 4954 (2005).
[63] J. B. Anderson, J. Chem. Phys. **63,** 1499 (1975).
[64] J. B. Anderson, J. Chem. Phys. **65,** 4121 (1976).
[65] M. A. Suhm and R. O. Watts, Physics Reports **204,** 293 (1991).
[66] R. Kosloff and H. Tal-Ezer, Chem. Phys. Lett. **127,** 223 (1986).
[67] M. D. Feit and J. A. Fleck, J. Chem. Phys. **78,** 301 (1983).
[68] V. Buch, J. Chem. Phys. **97,** 726 (1992).
[69] H.-S. Lee, J. M. Herbert, and A. B. McCoy, J. Chem. Phys. **111,** 9203 (1999).
[70] D. M. Benoit and D. C. Clary, J. Chem. Phys. **113**(13), 5193 (2000).
[71] H.-S. Lee and A. B. McCoy, J. Chem. Phys. **114,** 10278 (2001).
[72] X. Huang, S. Carter, and J. M. Bowman, J. Chem. Phys. **118**(12)**,** 5431 (2003).
[73] J. Koput, S. Carter, and N. C. Handy, J. Chem. Phys. **115,** 8345 (2001).
[74] X. Huang, S. Carter, and J. M. Bowman, private communication.
[75] B. M. Auer and A. B. McCoy, J. Phys. Chem. A **107,** 4 (2003).
[76] S. Broude and R. B. Gerber, Chem. Phys. Lett. **258,** 416 (1996).
[77] P. Sandler, V. Buch, and J. Sadlej, J. Chem. Phys. **105,** 10387 (1996).
[78] P. Sandler, V. Buch, and D. C. Clary, J. Chem. Phys. **101,** 6353 (1994).
[79] H.-S. Lee, J. M. Herbert, and A. B. McCoy, J. Chem. Phys. **110,** 5481 (1999).
[80] P. Langfelder, S. M. Rothstein, and J. Vrbik, J. Chem. Phys. **107**(20)**,** 8526 (1997).
[81] D. Blume, M. Lewerenz, and K. B. Whaley, J. Chem. Phys. **107,** 9067 (1997).
[82] P. H. Acioli, L. S. Costa, and F. V. Prudente, J. Chem. Phys. **111**(14)**,** 6311 (1999).
[83] C. Eckart, Phys. Rev. **47,** 552 (1935).
[84] J. D. Louck and H. W. Galbraith, Rev. Mod. Phys. **48,** 69 (1976).
[85] P. F. Bernath, *Spectra of Atoms and Molecules* (Oxford, New York, 1995).
[86] D. F. Coker and R. O. Watts, Mol. Phys. **58**(6)**,** 1113 (1986).
[87] D. M. Ceperley and B. Bernu, J. Chem. Phys. **89,** 6316 (1988).
[88] S. Broude, J. O. Jung, and R. B. Gerber, Chem. Phys. Lett. **299**(5)**,** 437 (1999).
[89] A. R. Cooper, S. Jain, and J. M. Hutson, J. Chem. Phys. **98,** 2160 (1993).
[90] R. Mayrhofer and E. L. Sibert, Theor. Chim. Acta **92**(2)**,** 107 (1995).
[91] T. A. Miller, private communication.
[92] D. J. Nesbitt, private communication.
[93] A. B. McCoy, Chem. Phys. Lett. **321,** 71 (2000).
[94] D. L. Crittenden, K. C. Thompson, M. Chebib, and M. J. T. Jordan, J. Chem. Phys. **121**(20)**,** 9844 (2004).